Electronic Supporting Information

Constructing the Square-Like Copper Cluster to Boost C-C Coupling for CO_2 Electroreduction to Ethylene

Tiantian Zhao,[1] Tingyu Yan,[1] Yuting Sun,[1] Zhongxu Wang, [1] Qinghai Cai,[1] Jingxiang Zhao[1,*] Zhongfang Chen[2,*]

[1] *College of Chemistry and Chemical Engineering, and Key Laboratory of Photonic and Electronic Bandgap Materials, Ministry of Education, Harbin Normal University, Harbin 150025, China*

[2] *Department of Chemistry, University of Puerto Rico, Rio Piedras Campus, San Juan, Puerto Rico 00931, USA*

[*] To whom correspondence should be addressed. Email: *zhaojingxiang@hrbnu.edu.cn (J. Z.).; zhongfang.chen1@upr.edu (Z.C.)*

COMPUTATIONAL DETAILS

The overpotential (η) for CO_2RR to C_2H_4 product can be obtained by the formula: $\eta = U_E - U_L$, where U_E is the equilibrium potential for C_2H_4 generation (0.06 V); U_L is the limiting potential (–0.32 V). Thus, η is 0.38 V.

The dissolution potential (U_{diss} = U° diss(bulk) – E_f/ne) is a good parameter to evaluate the electrochemical stability of metal doping, where U° diss(bulk), E_f, and n are the standard dissolution potential of bulk metal (0.34 V), the formation energy of the catalyst (0.76 V), and the number of electrons involved in the dissolution, respectively. In details, U_{diss} = (0.34 V – 0.76 eV/2e) = –0.04 V.

Table S1. The computed limiting potential (U_L, V) for the CO_2-to-C_2H_4 conversion in different solvation states.

Solvation	**U_L**
Without solvation	–0.32
Implicit Solvation	–0.30
Explicit Solvation	–0.35
Implicit Solvation + Explicit Solvation	–0.35

Table S2. Computed free energy changes (ΔG, in eV) for all potential elementary steps involved in the CO_2 electroreduction (CO_2ER) on the Cu_5@MoS_2 catalyst. Favorable steps are highlighted in red.

Elementary step on Cu_5@MoS_2	ΔG
$^* + CO_2 + H^+ \rightarrow {}^*COOH$	0.22
$^*COOH + H^+ + e^- \rightarrow {}^*CO + H_2O$	0.19
$^*CO + CO \rightarrow {}^*C_2O_2$	-0.93
$^*C_2O_2 + H^+ + e^- \rightarrow {}^*C_2O_2H$	0.32
$^*C_2O_2 + H^+ + e^- \rightarrow {}^*COCHO$	0.48
$^*C_2O_2H + H^+ + e^- \rightarrow {}^*C_2O + H_2O$	-0.73
$^*C_2O_2H + H^+ + e^- \rightarrow {}^*COCHOH$	0.73
$^*C_2O_2H + H^+ + e^- \rightarrow {}^*COHCOH$	0.39
$^*C_2O_2H + H^+ + e^- \rightarrow {}^*CHOCOH$	0.67
$^*C_2O + H^+ + e^- \rightarrow {}^*CHCO$	0.10
$^*C_2O + H^+ + e^- \rightarrow {}^*C\text{-}COH$	1.23
$^*C_2O + H^+ + e^- \rightarrow {}^*C\text{-}CHO$	0.15
$^*CHCO + H^+ + e^- \rightarrow {}^*CHCHO$	-0.36
$^*CHCO + H^+ + e^- \rightarrow {}^*CHCOH$	0.14
$^*CHCO + H^+ + e^- \rightarrow {}^*CH_2CO$	0.05
$^*CHCHO + H^+ + e^- \rightarrow {}^*CHCHOH$	0.22
$^*CHCHO + H^+ + e^- \rightarrow {}^*CHCH_2O$	0.36
$^*CHCHO + H^+ + e^- \rightarrow {}^*CH_2CHO$	0.70
$^*CHCHOH + H^+ + e^- \rightarrow {}^*CHCH + H_2O$	-0.12
$^*CHCHOH + H^+ + e^- \rightarrow {}^*CHCH_2OH$	0.37
$^*CHCHOH + H^+ + e^- \rightarrow {}^*CH_2CHOH$	0.13
$^*CHCH + H^+ + e^- \rightarrow {}^*CH_2CH$	0.13
$^*CH_2CH + H^+ + e^- \rightarrow {}^*CH_2CH_2$	-0.25
$^*CH_2CH_2 \rightarrow CH_2CH_2 + {}^*$	0.22

Table S3. The quadratic relation between the energy (E) of the reaction intermediates and their dependence on the applied electrochemical potential (U).

Reaction intermediates	Energy (E)	R^2
*	$E = -0.96U^2 - 1.03U - 364.96$	0.99
$^*CO$	$E = -1.35U^2 - 1.11U - 380.62$	0.99
$^*C_2O_2$	$E = -1.08U^2 + 0.01U - 396.25$	0.99
$^*C_2O_2H$	$E = -0.91U^2 - 0.49U - 400.41$	0.99
$^*C_2O$	$E = -1.04U^2 - 0.88U - 390.14$	0.99
$^*CHCO$	$E = -0.94U^2 - 0.50U - 393.55$	0.99
$^*CHCHO$	$E = -1.00U^2 - 0.67U - 397.83$	0.99
$^*CHCHOH$	$E = -0.92U^2 - 0.74U - 401.44$	0.99
$^*CHCH$	$E = -0.97U^2 - 1.04U - 390.23$	0.99
$^*CH_2CH$	$E = -1.20U^2 - 0.82U - 393.40$	0.99
$^*CH_2CH_2$	$E = -1.00U^2 - 1.14U - 397.88$	0.99

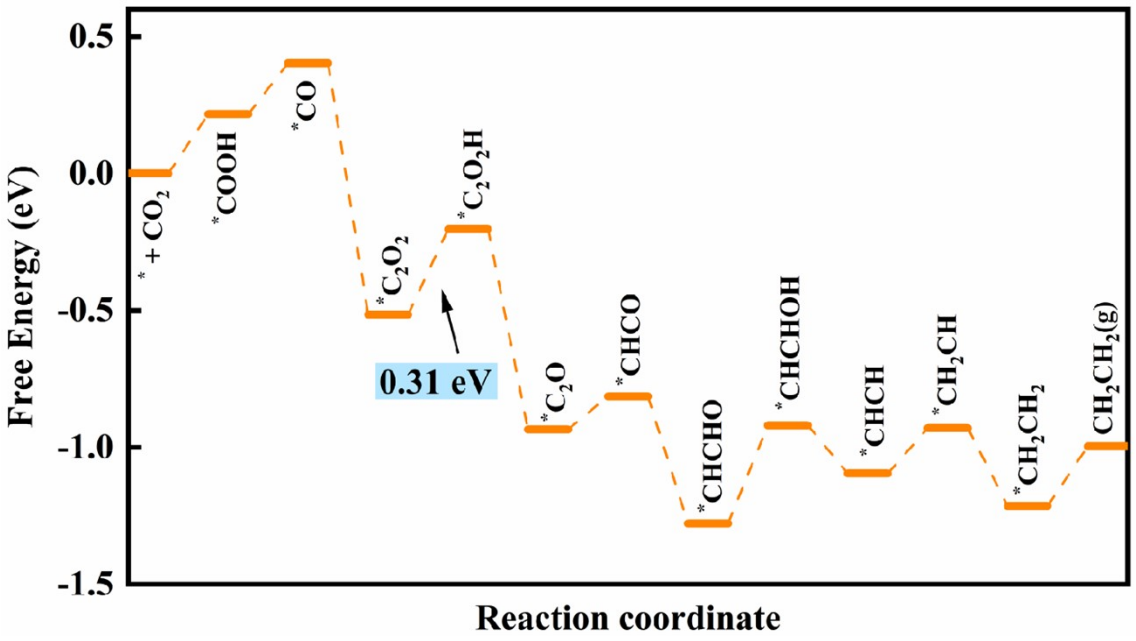

Fig. S1. The computed free energy profile for the CO_2ER to C_2H_4 production on Cu_5/MoS_2 catalyst by using the revised Perdew-Burke-Ernzerhof (rPBE) functional.

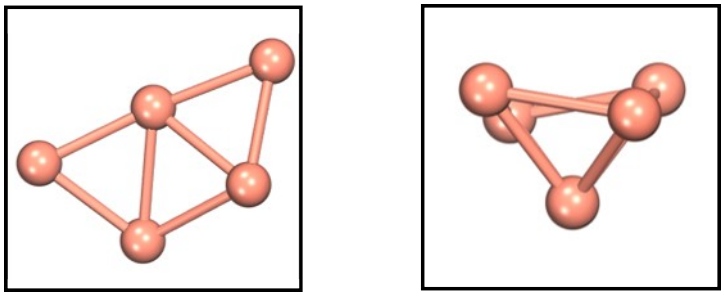

(a)

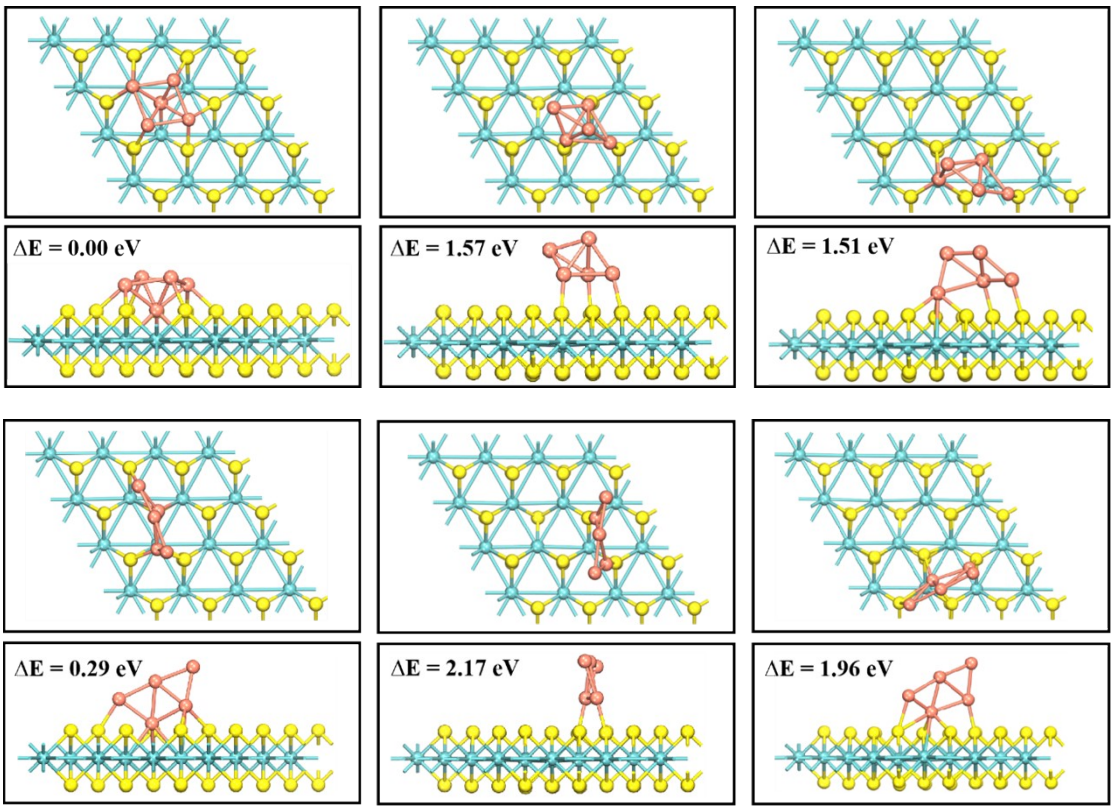

(b)

Fig. S2. (a) Optimized configurations of the planar and three-dimensional (3D) Cu_5 clusters. (b) Optimized configurations of the two Cu_5 clusters on different initial sites, along with their relative energies difference (ΔE).

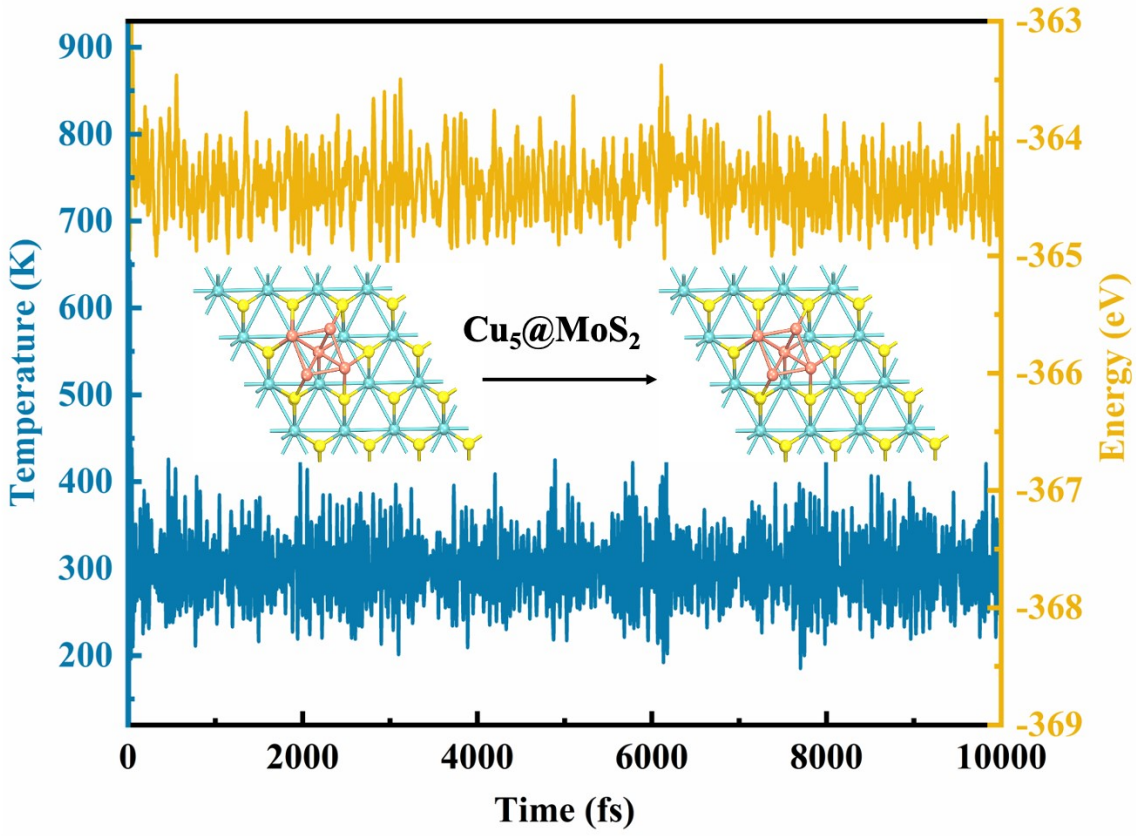

Fig. S3. Variations of temperature and energy as a function of the time for AIMD simulations of a 4 × 4 supercell Cu_5@MoS_2 for 20 *ps* with a time step of 2 *fs*.

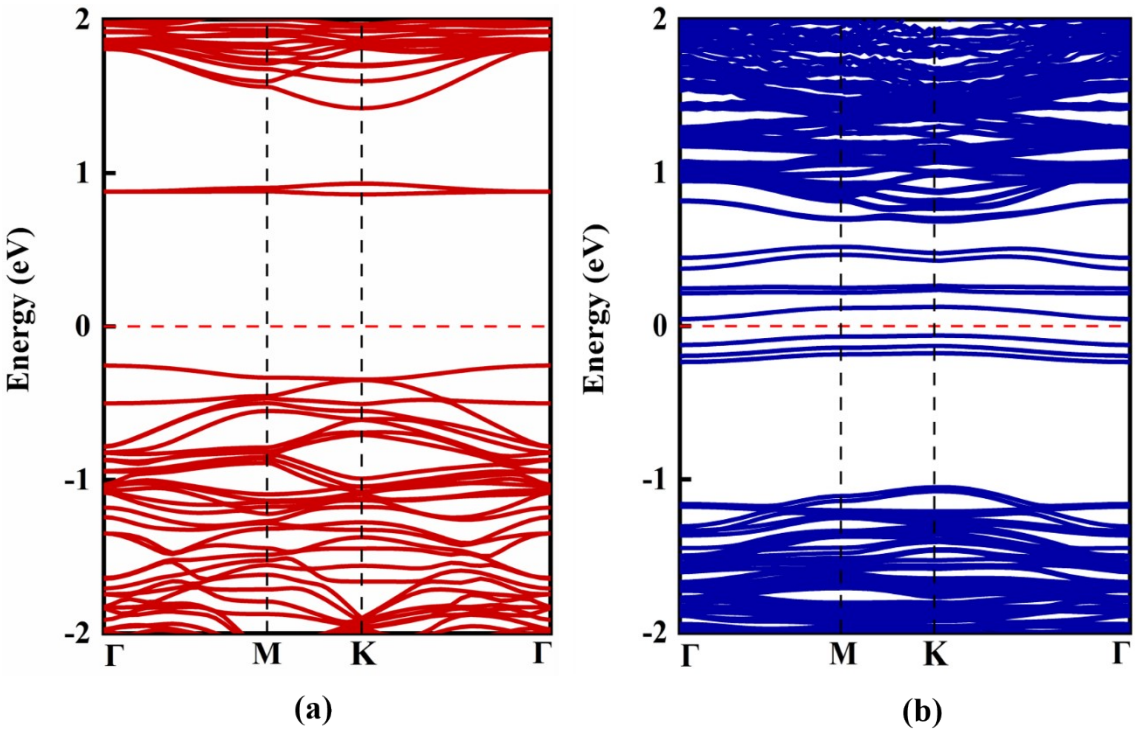

Fig. S4. Computed band structures of (a) the defective MoS_2 monolayer and (b) the Cu_5@MoS_2 catalyst. The Fermi level was set to zero in a dotted red line.

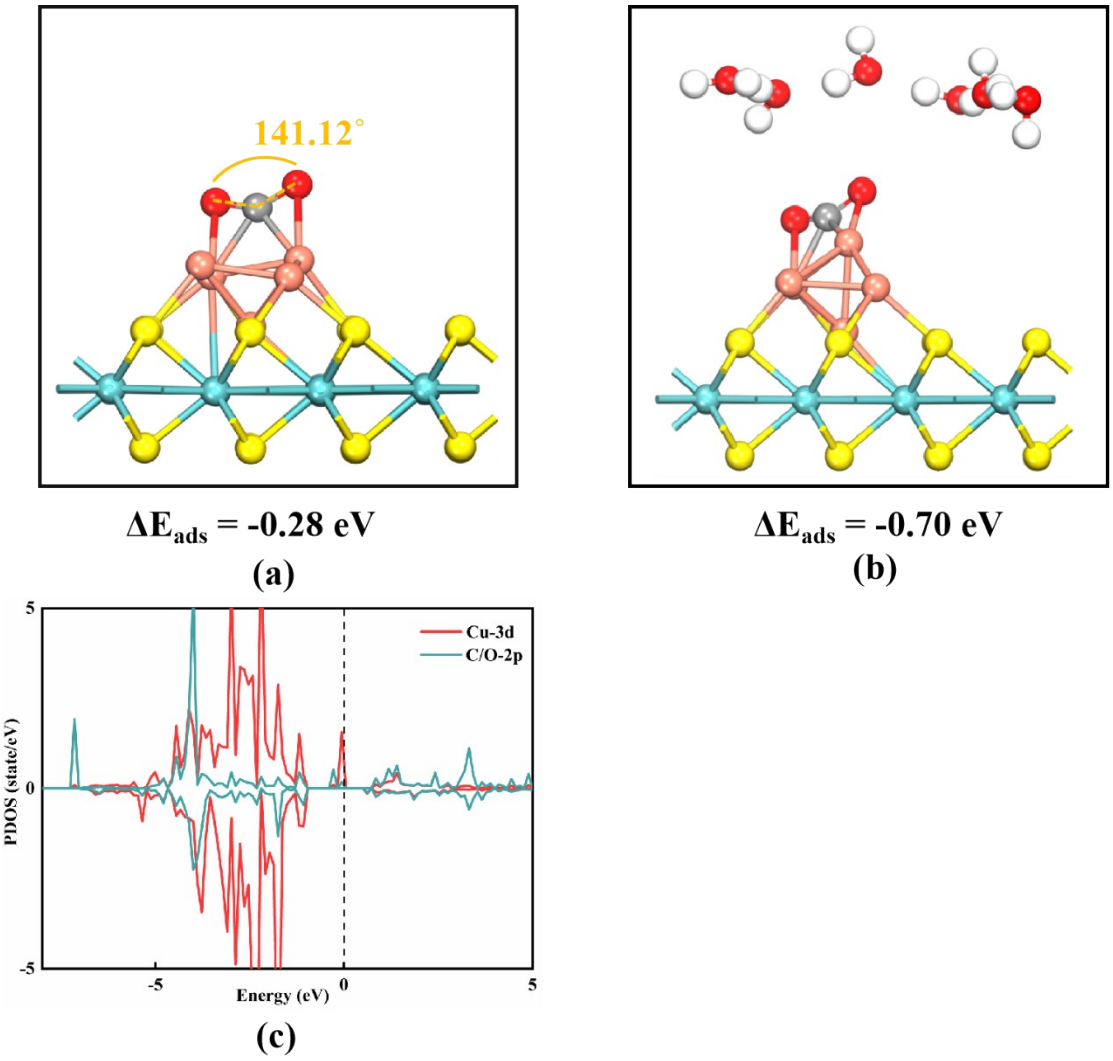

Fig. S5. Optimized $^{*}CO_2$ adsorption structures on the Cu_5@MoS_2 catalyst (a) without (b) with explicit solvent, (c) hybridization between C-2p/O-2p orbitals and Cu-3d orbitals.

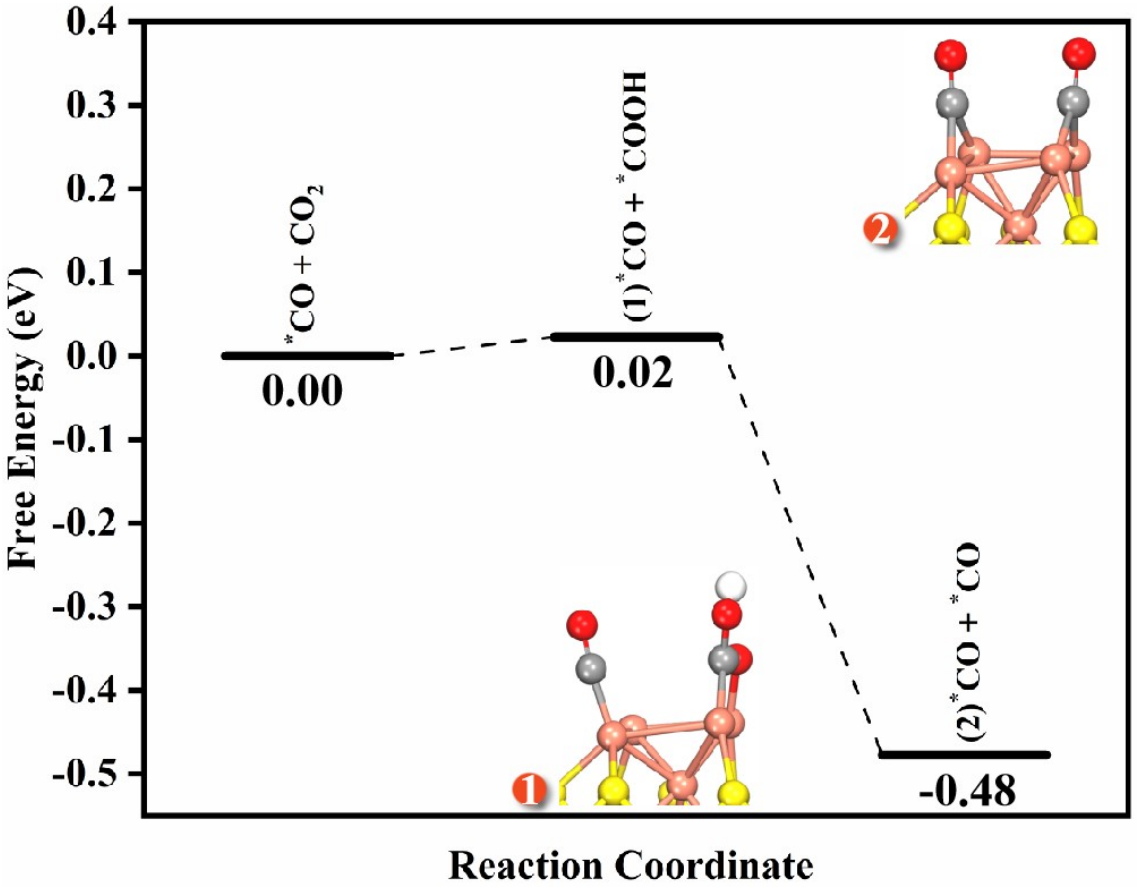

Fig S6. The computed free energy diagram illustrating the reaction pathway from *CO + CO_2 to *CO + *CO on the Cu_5@MoS_2 surface, including the relevant reaction intermediates.

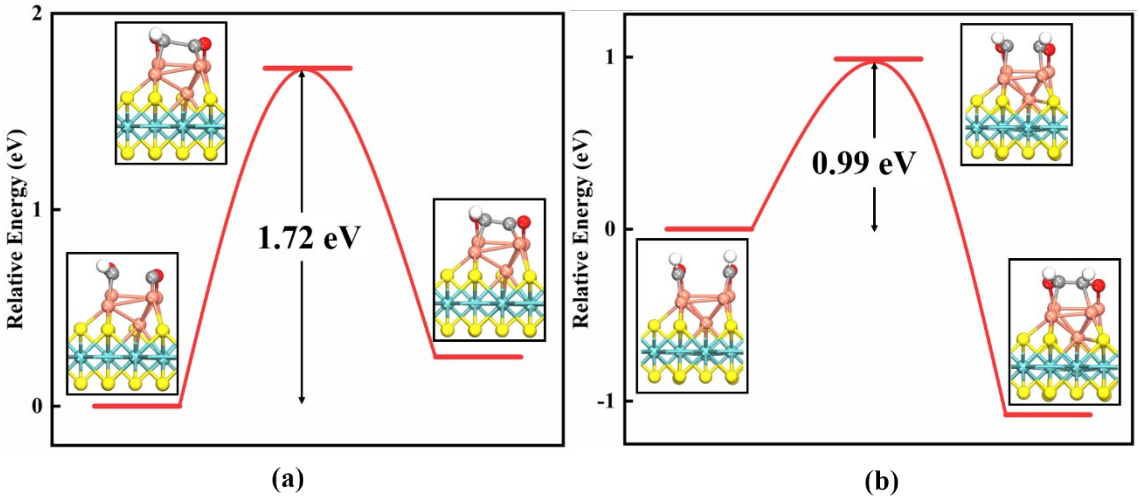

Fig. S7. The minimum-energy reaction paths for (a) *CHO + *CO, and (b) *CHO + *CHO on the Cu_5@MoS_2 catalyst.

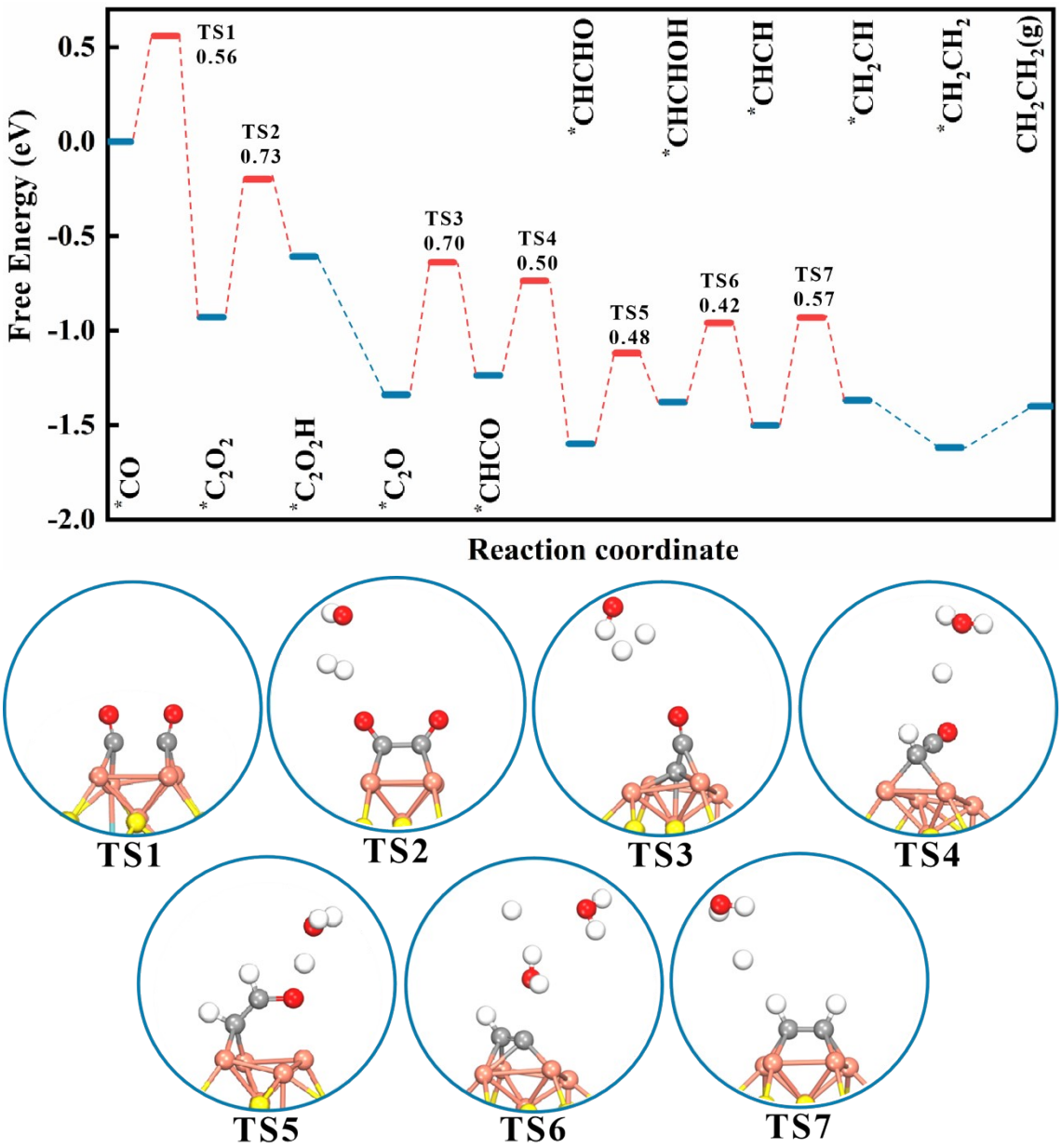

Fig. S8. The computed minimum energy path for CO_2RR to C_2H_4, and the corresponding structures of various transition states (TSs).

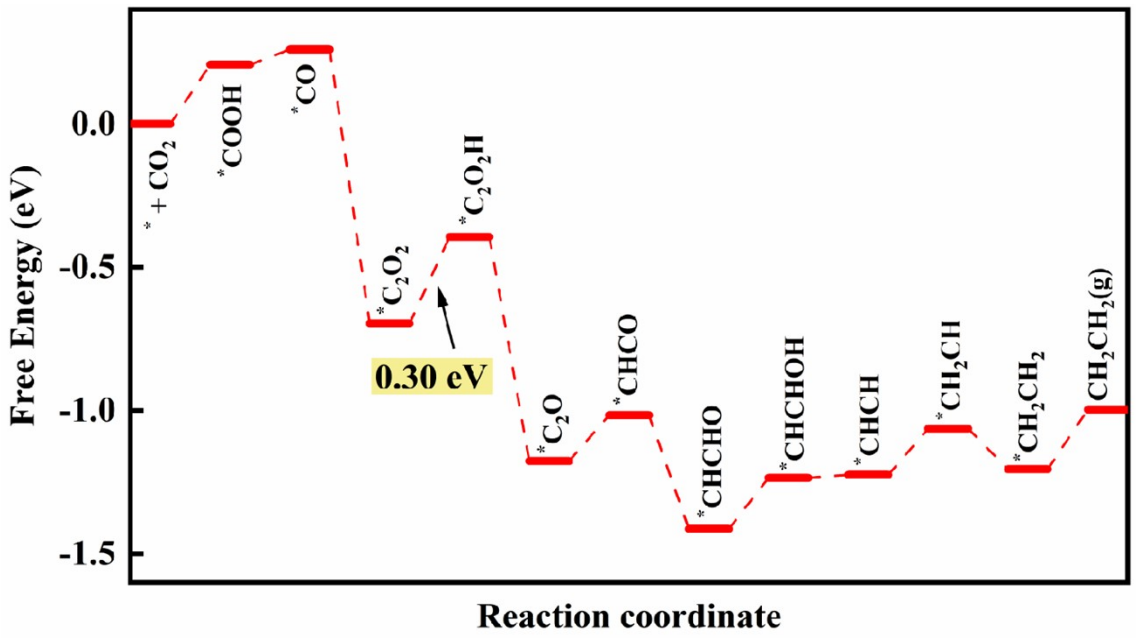

Fig. S9. The solvent effect on the catalytic activity of the design Cu_5/MoS_2 catalyst.

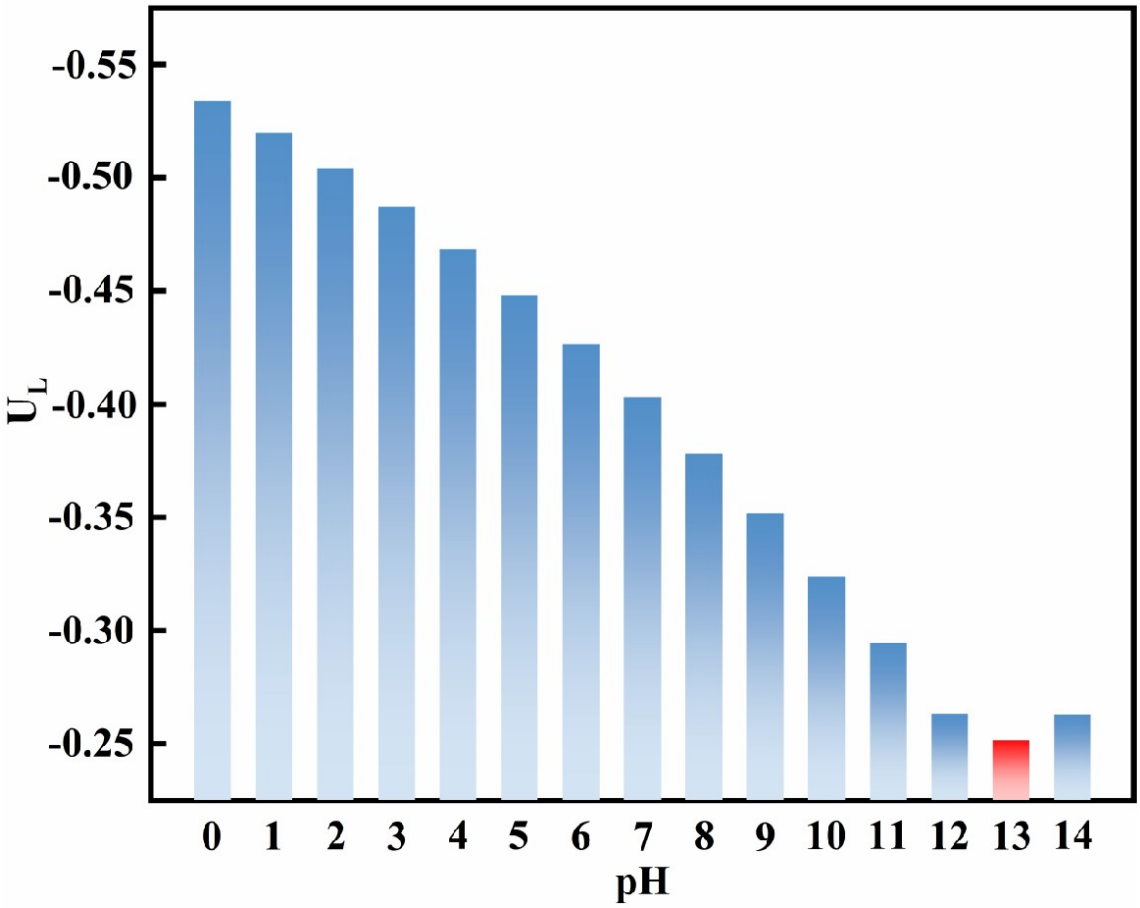

Fig. S10. Computed limiting potentials (U_L) for CO_2ER to C_2H_4 on the Cu_5@MoS_2 surface at different pH values.

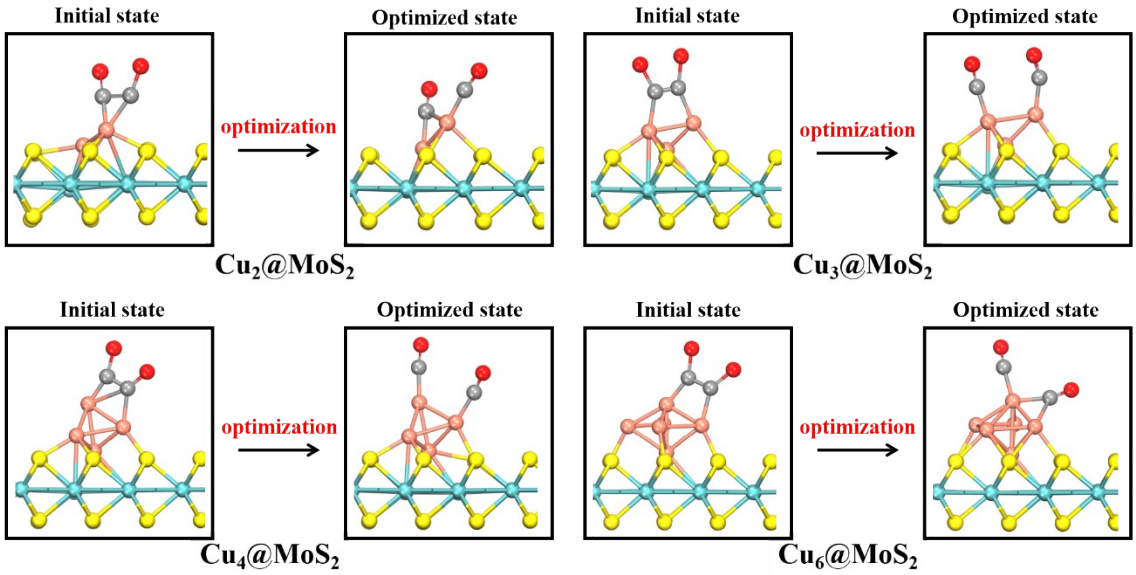

(a)

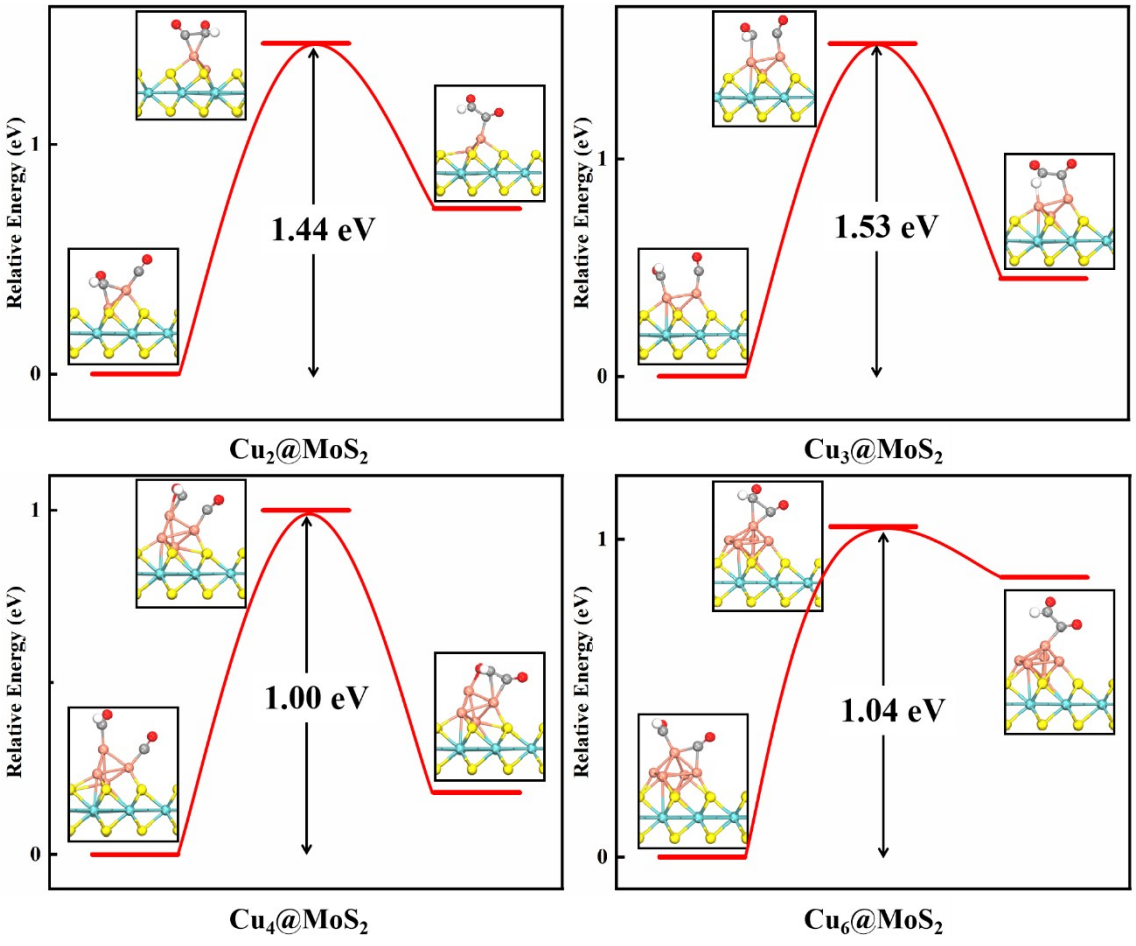

(b)

Fig. S11. (a) Two isolated CO species after full structural relaxation and (b) minimum-energy reaction paths for *CHO + *CO on $Cu_2@MoS_2$, $Cu_3@MoS_2$, $Cu_4@MoS_2$, and $Cu_6@MoS_2$ catalysts.